

# Machine learning classification: case of Higgs boson CP state in $H \rightarrow \tau\tau$ decay at LHC

K. Lasocha<sup>a,b</sup>, E. Richter-Was<sup>a</sup>, D. Tracz<sup>a,\*</sup>, Z. Was<sup>c</sup> and P. Winkowska<sup>d,\*</sup>

<sup>a</sup> *Institute of Physics, Jagellonian University, ul. Łojasiewicza 11, 30-348 Kraków, Poland*

<sup>b</sup> *CERN, 1211 Genewa 23, Switzerland*

<sup>c</sup> *IFJ-PAN, 31-342, ul. Radzikowskiego 152, Kraków, Poland*

<sup>d</sup> *Department of Computer Science, AGH USiT, Al. Mickiewicza 30, 30-059 Kraków, Poland*

## ABSTRACT

The Machine Learning (ML) techniques are rapidly finding their place as standard methods of the data analysis in High Energy Physics. In this paper we continue discussion on their application to measurement of the CP state of the Higgs boson discovered by Large Hadron Collider experiments at CERN laboratory in 2012.

We consider measurement in the  $H \rightarrow \tau\tau$  decay channel and use ML techniques to discriminate between models based on variables defined in the multi-dimensional phase-space. We discuss and quantify possible improvements for the two most sensitive decay modes:  $\tau^\pm \rightarrow \rho^\pm \nu$  with  $\rho^\pm \rightarrow \pi^\pm \pi^0$  and  $\tau^\pm \rightarrow a_1^\pm \nu$  with  $a_1^\pm \rightarrow \rho^0 \pi^\pm \rightarrow 3\pi^\pm$ .

In previous publications information on the hadronic decay products of the  $\tau$  leptons was used. Discriminating between Higgs boson CP state was studied as binary classification problem. Now we show how approximate constraints on the outgoing neutrinos momenta, not accessible in a direct way, can help to improve classification performance. Added to the ML classification features significantly enhance the sensitivity for Higgs boson CP state. In principle all information is provided with 4-momenta of the final state particles present in the events. As we have observed in the past, not all of such information is straightforward to be identified in ML training. We investigate how optimised high-level features, like some angles of neutrino orientation, may improve ML results. This can be understood as an intermediate step toward choice of better classifiers where expert variables will not be necessary.

For the performance comparison, in parallel to *Deep Learning Neural Network*, we use other ML methods: *Boosted Trees*, *Random Forest* and *Support Vector Machine*.

IFJPAN-IV-2018-20 December 2018

---

(\*) In time of working on this project.

This project was supported in part from funds of Polish National Science Centre under decisions DEC-2017/27/B/ST2/01391. DT and PW were supported from funds of Polish National Science Centre under decisions DEC-2014/15/B/ST2/00049.

Majority of the numerical calculations were performed at the PLGrid Infrastructure of the Academic Computer Centre CYFRONET AGH in Krakow, Poland.

# 1 Introduction

Machine Learning (ML) techniques find increasing number of applications in the domain of High Energy Physics phenomenology, where several tasks require classification in high-dimensional variable space. For the comprehensive recent review see [1]. Over the last years the most significant progress with new ML techniques was made in hadronic jets reconstruction and classification: mass reconstruction, jet substructure, jet-flavour and charge classification. They are very important benchmarks and long standing challenges for more classical algorithms. Example of such recent analyses can be found in Refs. [2, 3, 4, 5].

Typical measured experimental sample consists of observed events. Each event can be understood as a point in multi-dimensional coordinate space, representing four-momenta and flavours of observed particles or group of particles. The physics goal is to identify properties of distributions constructed from these events and interpret in physically meaningful way. The ML algorithms with the low-level features of the event sample are not necessarily able to capture efficiently all information available in the data. The most performing strategy seems still to be mixing of low-level information with the human-derived high-level features, based on the physics insight into the problem. Examples of such analyses are presented in [6, 7]. The strategy of mixing low-level and high-level features, prepared to remove trivial (physics-wise) symmetries are explored successfully there. The ML algorithm does not need to learn some basic physics rules, like rotation symmetry of the observables. It is of importance how features need to be prepared for the input to ML algorithms.

In previous paper [8] we have demonstrated that ML methods, like *Deep Learning Neural Network* (DNN) [9], can be a promising analysis method to constrain Higgs parity in decay channel  $H \rightarrow \tau\tau$ . We considered two decay modes of the  $\tau$  leptons:  $\tau^\pm \rightarrow \rho^\pm \nu$ ,  $\tau^\pm \rightarrow a_1^\pm \nu$ , followed by  $\rho^\pm \rightarrow \pi^\pm \pi^0$  and  $a_1^\pm \rightarrow \rho^0 \pi^\pm \rightarrow 3\pi^\pm$ . This forms three possible final state configurations of interest from the decay of  $\tau$ -pair:  $\rho^\pm \rho^\mp$ ,  $a_1^\pm \rho^\mp$  and  $a_1^\pm a_1^\mp$ , each accompanied by  $\tau$  neutrino pair. The  $a_1^\pm, \rho^\mp$  intermediate resonances decay further into mixture of  $\pi^\pm, \pi^0$ :  $a_1^\pm \rightarrow \pi^0 \pi^\pm \rightarrow 3\pi^\pm$ ,  $\rho^\pm \rightarrow \pi^\pm \pi^0$ . The information about Higgs boson CP state is encoded in the angles between outgoing decay products and angles between intermediate resonance decay planes. From previous studies [10, 11] performed with more classical optimal observables, we have observed that the best discrimination was achievable from features constructed in the rest frame of the primary intermediate resonance pair rotated to align direction of the outgoing resonances with the  $z$ -axis. This idea was explored also in [8] and will be followed in this paper. We have investigated inputs of mixed low-level and high-level features. Many of high-level features turned out to be finally not necessary, but provided nevertheless benchmark results. On the other-hand (post-fact seemingly simple) preparation of some low-level features was necessary to achieve any significant result.

In paper [8] we have limited analysis to studies on the ML potential for discriminating between different Higgs CP hypotheses, with input information from 4-momenta of the hadronic decay products,  $\pi^\pm, \pi^0$ , no detector effects taken into account. The study was followed by a more systematic evaluation within context of experimental analysis [12]. The conclusions on the ML method performance survived and we will not repeat this evaluation in scope of the paper.

As pointed already in [13] every  $\tau$  decay should have the same sensitivity to  $\tau$  spin. That is why, from the results presented in [8], it is clear that there is a sizable sensitivity left out with the information on the neutrino momenta. Our past studies did not rely on the neutrinos because they can not be measured directly. However one can reconstruct the neutrino momenta with some approximations from kinematics of hadronic decay products and other information available experimentally on the whole event. In particular, partial reconstruction of the  $\tau$  decay vertex position is possible. This brings new challenges and new opportunities which we will explore with the help of *expert variables*: the azimuthal angles of neutrino orientation. The encouragement, that the information may become experimentally available with adequate precision, can be deduced e.g. from reports by ATLAS Collaboration [14, 15] on the  $H \rightarrow \tau\tau$  signal measurement and on the B meson decay vertex position.

In the present studies we investigate how to reconstruct neutrinos four momenta from measurable quantities and quantify under which conditions such approximate information can be useful. The proposed scenario consists of 3 steps:

1. reconstruction from constraint of missing transverse energy of the whole event  $E_{miss}^x, E_{miss}^y$  and from invariant mass of the Higgs boson  $m_H$ , of neutrino 4-momenta components collinear to directions of visible decay products of  $\tau$  leptons,
2. reconstruction from constraint of the  $\tau$  lepton invariant mass  $m_\tau$ , modules of transverse components for neutrino momenta,

3. reconstruction of two remaining azimuthal angles of the neutrinos with the help of  $\tau$ -decay vertices positions.

The goal is to reconstruct 6 quantities: the  $x, y, z$  components of neutrino and anti-neutrino momenta. After step (1) we have 4 independent variables still to constrain, after step (2) it reduces to two. The burden of building constraints from the decay vertex position, which is probably least precise to measure, is minimized. This approach can be understood as an attempt to construct high-level feature with expert supported design. This if useful, may be later replaced with non-sub-optimal choices. Several papers followed such strategy [16, 17, 18] having in mind approach of optimal variables.

Similarly as in [8] we perform DNN analysis for three decay modes of the  $\tau$  lepton pairs, which will be denoted respectively as:  $\rho^\pm - \rho^\mp$ ,  $a_1^\pm - \rho^\mp$  and  $a_1^\pm - a_1^\mp$ . Two hypotheses of Higgs parity states are confronted only. However extension to parametrised classification, similar to approach taken in [19], could be envisaged as an obvious next step; the measurement of the Higgs CP parity mixing angle. Our paper can be understood as an exercise into that direction.

Our base-line for ML method is the DNN, nonetheless we have also worked with more classical techniques like *Boosted Trees* (BT) [20], *Random Forest* (RF) [21] and *Support Vector Machine* (SVM) [22]. The DNN technique by far outperforms all of them. This comparative analysis, rely on the  $\rho^\pm - \rho^\mp$  case.

Our paper is organised as follows. In Section 2 we briefly recall results from previous studies of Ref. [8]. In Section 3 we discuss how to reconstruct, with some approximation, information on the outgoing neutrinos momenta. We evaluate information from the decay vertices position relative to the production vertex. In Section 4 we present improvement in the DNN classification performance from information on the neutrinos. We quantify what would be the acceptable precision on azimuthal angle of two neutrinos, to still improve the performance of the classifier. Section 5 summarizes main results and give outlook on the possible further progress.

In Appendix A details concerning DNN analysis implementation are given. In Appendix B results achieved on the same problem but with different ML techniques: BDT, RF and SVM are presented. We discuss technical performance, like usage of CPU or transient memory too.

## 2 Classification based on hadronic decay products

Let us comment briefly on a few selected results from paper [8], summarized in Table 1. For the ML classification directly measurable 4-momenta of the hadronic decay products of the  $\tau$  leptons were considered only. They were boosted into the rest-frame of the primary intermediate resonance pairs, respectively  $\rho^\pm - \rho^\mp$ ,  $a_1^\pm - \rho^\mp$  or  $a_1^\pm - a_1^\mp$ . All four vectors were later rotated to the frame where primary resonance momentum 3-vectors were set along  $z$ -axis. It greatly improved learning process, as the ML algorithm did not have e.g. to rediscover rotation symmetry. In particular, from the very beginning internal weights of the ML algorithms could use transverse CP sensitive degrees of freedom separated from the longitudinal ones to differentiate among events. To classify performance for Higgs parity identification a weighted Area Under Curve (AUC) [23, 24] was used. The score of true classification (oracle predictions) for this problem is 0.782, independently<sup>1</sup> of the decay mode, while random classification corresponds to 0.500. The achieved ML performance was between 0.557 - 0.638, depending on the  $\tau$ -pair decay channels.

Note, that this much lower than oracle classification is due to missing information on the neutrino momenta, not accesible directly for experimental measurement, but which are important carriers of the spin information. Let us explain very briefly the physics context of the problem. Higgs boson Yukawa coupling expressed with the help of the scalar–pseudoscalar mixing angle  $\phi$  reads  $N \bar{\tau}(\cos\phi + i\sin\phi\gamma_5)\tau$  where  $N$  denotes normalization and  $\bar{\tau}, \tau$  spinors of the  $\tau^+$  and  $\tau^-$ . We follow notation of Ref. [25]. The matrix element squared for the scalar / pseudoscalar / mix parity Higgs, with decay into  $\tau^+\tau^-$  pairs can be expressed as follows

$$|M|^2 \sim 1 + h_+^i \cdot h_-^j R_{i,j}; \quad i, j = \{x, y, z\}. \quad (1)$$

The corresponding CP sensitive spin weight  $wt$  is rather simple:

$$wt = 1 - h_+^z h_-^z + h_+^\perp R(2\phi) h_-^\perp. \quad (2)$$

The formulae are valid for  $h_\pm$  defined in  $\tau^\pm$  rest-frames, the  $R(2\phi)$  denote the rotation matrix for  $2\phi$  around the  $z$  direction:  $R_{xx} = R_{yy} = \cos 2\phi$ ,  $R_{xy} = -R_{yx} = \sin 2\phi$ . The  $\tau^\pm$  decay polarimetric vectors  $h_+^i, h_-^j$ , in the simplest case

<sup>1</sup>This is a consequence of  $\tau$  decay dynamic. See e.g. Ref. [13].

Table 1: The ML performance for discriminating between scalar and pseudoscalar Higgs CP state, based on 4-vectors of hadronic decay products. Numbers taken from [8].

Line content	Decay mode: $\rho^\pm - \rho^\mp$ $\rho^\pm \rightarrow \pi^\pm \pi^0$	Decay mode: $a_1^\pm - \rho^\mp$ $a_1^\pm \rightarrow \rho^0 \pi^\pm, \rho^0 \rightarrow \pi^+ \pi^-$ $\rho^0 \rightarrow \pi^+ \pi^-$	Decay mode: $a_1^\pm - a_1^\mp$ $a_1^\pm \rightarrow \rho^0 \pi^\pm, \rho^0 \rightarrow \pi^+ \pi^-$
$H \rightarrow \tau\tau$ fraction	6.5%	4.6%	0.8%
Number of features	24	32	48
True classification (oracle)	0.782	0.782	0.782
ML classification	0.638	0.590	0.557

of  $\tau^\pm \rightarrow \pi^\pm \pi^0 \nu$  decay, can be expressed with the 4-momenta  $p_{\pi^\pm}, p_{\pi^0}, p_\nu$  of  $\tau$  decay products  $\pi^\pm, \pi^0$  and  $\nu_\tau$ :

$$h_\pm^i = \mathcal{N} \left( 2(q \cdot p_\nu) q^i - q^2 p_\nu^i \right). \quad (3)$$

The  $q = p_{\pi^\pm} - p_{\pi^0}$ . Obviously, part of the CP sensitivity can be extracted only if  $p_\nu$  is known. Note that spin weight  $wt$  is a simple first order trigonometric polynomial in a (doubled) Higgs CP parity mixing angle  $\phi$ . This form is preserved for all  $\tau$  decay channels.

### 3 Approximating components of neutrino momenta

We start with approximate neutrino momenta in the ultrarelativistic (collinear) approximation. We temporarily assume that neutrino momenta and visible  $\tau$  products momenta are collinear to each other. Later, we relax this oversimplification. This gives reasonable approximation for collinear components which are the largest ones (not only in the laboratory frame, but also in Higgs rest frame and the rest frame of its visible decay products). We will cover this construction in detail. Our conjecture is that some of these steps may be in the future replaced by the solutions present in the ML technique and our expert variables will not be needed.

#### 3.1 Collinear approximation

The basic kinematical constraint on 4-momenta of each  $\tau \rightarrow h\nu$  decay, where  $h$  stands for hadronic particles produced in decay reads:

$$p_{\tau_1} = p_{h_1} + p_{\nu_1}, \quad p_{\tau_2} = p_{h_2} + p_{\nu_2} \quad (4)$$

where  $p_{\tau_1}, p_{\tau_2}$  denote 4-vectors of decaying  $\tau$  leptons;  $p_{h_1}, p_{h_2}$  denote 4-vectors of their hadronic (i.e. measurable) decay products combined and  $p_{\nu_1}, p_{\nu_2}$  denote 4-vectors of corresponding to decays neutrinos.

We assume that direction of the hadronic decay products and neutrino are parallel to the direction of the decaying  $\tau$  and we can write for 3-vectors

$$\vec{p}_h = x \cdot \vec{p}_\tau, \quad \vec{p}_\nu = (1-x) \cdot \vec{p}_\tau, \quad (5)$$

where  $x$  is in the range (0,1). We can then express for the  $\tau^+$  and  $\tau^-$

$$\vec{p}_\nu = \frac{1-x}{x} \cdot \vec{p}_h = \alpha \cdot \vec{p}_h. \quad (6)$$

Applying equation (6) to both  $\tau^\pm$  we get the following relations

$$|\vec{p}_{\nu_1}| = \alpha_1 \cdot |\vec{p}_{h_1}|, \quad |\vec{p}_{\nu_2}| = \alpha_2 \cdot |\vec{p}_{h_2}|. \quad (7)$$

Relations hold both in the laboratory frame and in the rest frame of the hadronic decay products. This is a property of Lorentz transformations (boost and rotation) of ultrarelativistic particles. This feature allows to calculate  $\alpha_1, \alpha_2$  in the laboratory frame and then use the rest frame of the hadronic decay products which seem to be optimal for building expert input variables for ML classification, as discussed in [8].

There are few options how to calculate  $\alpha_1, \alpha_2$  from known 4-momenta of hadronic decay products and auxiliary information available in the event. We will discuss them below.

### 3.1.1 The $E_{miss}^x, E_{miss}^y$ constraints

The auxiliary information of the event, which can be used to constrain neutrino momentum, is imbalance in the laboratory frame of the event in the plane transverse to the beam direction, usually denoted as  $E_{miss}^x, E_{miss}^y$ . It is attributed to the sum of transverse components of the neutrino momenta, but it also accumulates all imperfections of the reconstruction of the other outgoing particles of that event, which add to event.

We assume validity of relation (6) and define

$$\begin{aligned} E_{miss}^x &= p_{\nu_1}^x + p_{\nu_2}^x = \alpha_1 \cdot p_{h_1}^x + \alpha_2 \cdot p_{h_2}^x, \\ E_{miss}^y &= p_{\nu_1}^y + p_{\nu_2}^y = \alpha_1 \cdot p_{h_1}^y + \alpha_2 \cdot p_{h_2}^y. \end{aligned} \quad (8)$$

Solving above equations one gets

$$\alpha_1 = \frac{E_{miss}^x - \alpha_2 \cdot p_{h_2}^x}{p_{h_1}^x} \quad (9)$$

and

$$\alpha_1 = \frac{E_{miss}^y - \alpha_2 \cdot p_{h_2}^y}{p_{h_1}^y}. \quad (10)$$

We can rearrange (9), (10) into expressions for  $\alpha_1$  and  $\alpha_2$ .

$$\begin{aligned} \alpha_2 &= \frac{E_{miss}^y \cdot p_{h_1}^x - E_{miss}^x \cdot p_{h_1}^y}{p_{h_2}^y \cdot p_{h_1}^x - p_{h_2}^x \cdot p_{h_1}^y}, \\ \alpha_1 &= \frac{E_{miss}^x - \alpha_2 \cdot p_{h_2}^x}{p_{h_1}^x}. \end{aligned} \quad (11)$$

We will use expressions (11) for the studies of ML classification.

### 3.1.2 Using $m_H$ constraint

Although equations (11) provide solution for both  $\alpha_1$  and  $\alpha_2$ , the  $E_{miss}^x, E_{miss}^y$  feature large experimental errors. High quality constraint from the known Higgs-boson and  $\tau$ -lepton masses is available, but it is not enough for both  $\alpha_1$  and  $\alpha_2$ . Only the product  $(1 + \alpha_1) \cdot (1 + \alpha_2)$  can be controlled

$$m_H^2 = (p_{\tau_1} + p_{\tau_2})^2 = 2 \cdot m_\tau^2 + 2 \cdot (1 + \alpha_1) \cdot (1 + \alpha_2) [E_{h_1} E_{h_2} - p_{h_1}^x \cdot p_{h_2}^x - p_{h_1}^y \cdot p_{h_2}^y - p_{h_1}^z \cdot p_{h_2}^z]. \quad (12)$$

We obtain

$$(1 + \alpha_1) \cdot (1 + \alpha_2) = \frac{m_H^2/2 - m_\tau^2}{E_{h_1} E_{h_2} - p_{h_1}^x \cdot p_{h_2}^x - p_{h_1}^y \cdot p_{h_2}^y - p_{h_1}^z \cdot p_{h_2}^z}. \quad (13)$$

The  $E_{h_1}, E_{h_2}$  denote energies of the hadronic systems  $h_1$  and  $h_2$ . For completeness and for later use, the  $E_\nu$  denote neutrino energy.

### 3.1.3 Choosing optimal solution for longitudinal neutrino momentum

We have at our disposal three independent equations: formulae of (11) and (13) to constrain two parameters  $\alpha_1, \alpha_2$ . We have checked that all three options:

- *Approx-1* : formulae (11) only,
- *Approx-2* : formula (13) and  $\alpha_1$  from formulae (11),
- *Approx-3* : formula (13) and  $\alpha_2$  from formulae (11),

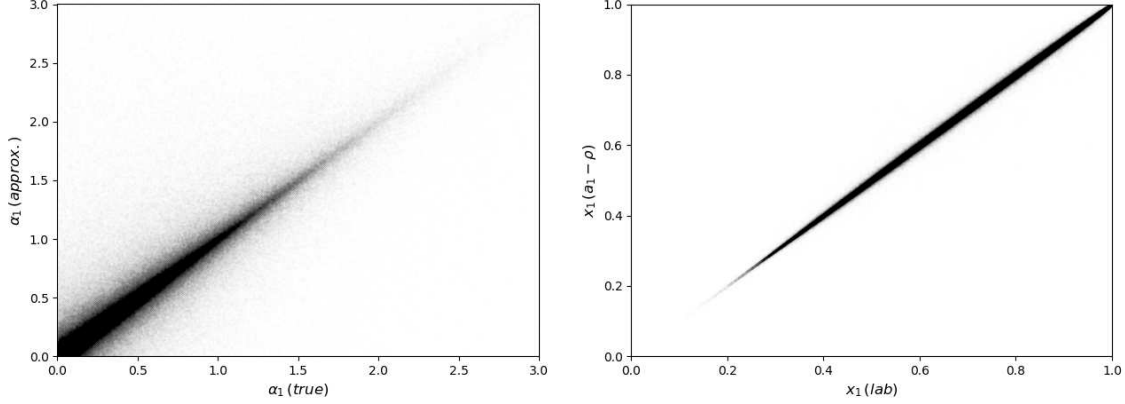


Figure 1: Left: Correlation between true and approximated  $\alpha_1$  calculated for the  $a_1^\pm - \rho^\mp$ . Right: Correlation between fraction  $x$  of  $\tau$  lepton momentum carried by hadronic decay products, in the *Approx-1* approximation in the  $a_1^\pm - \rho^\mp$  and laboratory frames.

lead to very comparable predictions and marginal differences in the ML performance. At least as long as smearing on the  $E_{miss}^x, E_{miss}^y$  is not imposed. It will be the main concern on experimental precision achievable with collinear approximation. We will not discuss experimental context, the option *Approx-1* will be used as a base-line for the results<sup>2</sup>.

To illustrate effectiveness, we show in Fig. 1 (left-plot) correlations between  $\alpha_1$ -true and  $\alpha_1$ -approximated, calculated for the  $a_1^\pm - \rho^\mp$  case. As a consistency check in Fig. 1 (right-plot) we show also correlations of  $x_1$ , calculated back from  $\alpha_1$  in the  $a_1^\pm - \rho^\mp$  rest frame and in laboratory frames. Sample of  $10^6$  events was used for these scattergrams.

### 3.2 Energy and transverse component of neutrino momenta

Now, we can use the knowledge of longitudinal (along visible decay products) component of neutrino momentum,  $p_V^z$ , and continue to constrain other components. In the rest frame of the hadronic decay products, the  $p_{h1,2}$  momenta are aligned with  $z$  direction:  $p_h^x = p_h^y = 0$ . We approximate modules of transverse neutrino momenta using as an input mass of  $\tau$  and visible decay products of each  $\tau$  lepton

$$m_\tau^2 = (E_V + E_h)^2 - (p_V^x)^2 - (p_V^y)^2 - (p_V^z + p_h^z)^2. \quad (14)$$

Massless neutrino gives us another constrain

$$0 = (E_V)^2 - |p_V^T|^2 - (p_V^z)^2. \quad (15)$$

Equations simplify to the following relations

$$\begin{aligned} E_V &= \frac{m_\tau^2 - E_h^2 + (p_h^z)^2 + 2 \cdot p_V^z p_h^z}{2E_h}, \\ p_V^T &= \sqrt{E_V^2 - (p_V^z)^2}, \end{aligned} \quad (16)$$

where  $p_V^z = \alpha \cdot p_h^z$  is calculated for one of the approximations for  $\alpha$  introduced in Section 3.1.3.

The  $\alpha_1, \alpha_2, E_{V1}$  and  $E_{V2}$  must be positive. Otherwise events are rejected. Also events, where approximated  $(p_V^T)^2$  are negative were rejected. In total, about 17% events are rejected from the sample when constructing neutrino momenta with the *Approx-1* option. Additional 11% is rejected when for a given event also calculations

<sup>2</sup>This point may become important for discussion of ambiguities due to missing  $p_T$  of jets accompanying the Higgs production. Then, it may be helpful to have 3 constraints which may be used e.g. for missing  $p_T^{miss}$  generated by jets, with heavy flavour resonances of decays with neutrinos, contributing to  $E_T^{miss}$  as well.



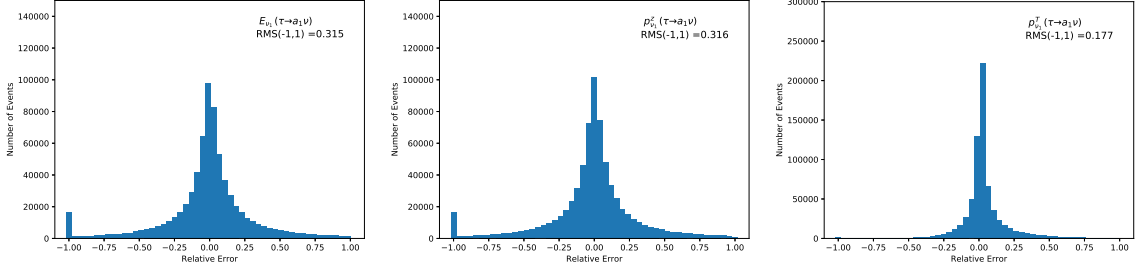


Figure 2: Distribution of the  $(x_{true} - x_{approx.})/x_{true}$  for the energy, longitudinal and transverse momenta of neutrino, approximated according to *Approx-1*. Events with relative error outside  $\pm 1.0$  window are cumulated in a bin at -1.0. Root Mean Square (RMS) is calculated in the range (-1.0, 1.0).

with *Approx-2* and *Approx-3* are requested to fulfil the above criteria. In Fig. 2 resolution distribution of calculated  $E_v, p_v^z, p_v^T$  for  $a_1^\pm - \rho^\mp$  is shown. The  $p_v^T$  is approximated with better resolution than  $E_v, p_v^z$ .

We keep in mind that for ML techniques, even approximate observables (expert variables) may be useful to improve classification scores.

### 3.3 Azimuthal angles of neutrinos

At this point, we are left with no approximation for two azimuthal angles for orientation of  $p_{v_1}^T$  and  $p_{v_2}^T$ . To capture the sensitivity of the Higgs boson CP, they have to be known in the rest frame of the visible  $\tau$  decay products. Those two angles can be inferred in the laboratory frame from the  $\tau$  decay vertices positions and then through known already parameters of boosts and rotations related to the one of visible decay products frame.

The measurement of  $\tau$  decay vertices is possible, because due to short, but nonetheless non-negligible lifetime of the  $\tau$  leptons, position of  $\tau$  decay does not coincide with the original  $pp$  collision point. The transverse coordinates of primary interaction point are to a good precision consistent with zero. At the same time, the tracks of the  $\tau$  decay products will not point to this interaction point but to shifted by  $\tau$  flight over its lifetime position of the  $\tau$  decay vertex. The direction of  $\tau$  flight can be thus reconstructed in part and as a consequence proportion of its momentum components. This provides constraint on  $v_\tau$  momentum as well. We do not intend to go into details of this challenging measurement of the secondary vertex position. Let us point to the Ref. [15], which discuss such measurement in the context of reconstructing secondary vertex in case of B-meson decay and its application for classification of hadronic jets originating from it. One can assume that such measurement is possible and orientation of  $v_\tau$  momentum around direction of visible hadronic  $\tau$  decay products, can be constrained.

To access how precisely we need to know this information, we take true azimuthal angles  $\phi_{v_1}, \phi_{v_2}$  in the rest frame of visible decay products and smear. For  $\Delta\phi_v = |\phi_v^{smeared} - \phi_v^{true}|$ , our smearing function  $f(\Delta\phi_v, \beta)$  reads simply

$$f(\Delta\phi_v, \beta) = \frac{1}{\beta} \exp\left(-\frac{1}{\beta} \Delta\phi_v\right), \quad (17)$$

with randomly generated sign of the shift added. We have chosen exponential shape, instead of often used in such cases gaussian shape, rather arbitrarily. Note however, that the length of  $\tau$  flight path follows exponential distribution.

## 4 Classification with DNN

The structure of the data and neural network architecture follows what was published in [8]. In fact, we use the same simulated samples and start from the code published there. The technical description on our DNN model is delegated to Appendix A.

Simulated data consist of events where all decay products are present with their flavours and four-momenta in a laboratory frame which are then transformed to respective rest frames as explained in Section 2. With respect to analysis published in [8] we explore approximate information on neutrino momenta derived from the kinematical

Table 2: List of features for ML classification, organised in the families of Variant-X.Y. In the third column number of features for the  $\rho^\pm - \rho^\mp$ ,  $a_1^\pm - \rho^\mp$  and  $a_1^\pm - a_1^\mp$  channels are given. All components of 4-vectors are calculated in the hadronic decay products rest frame. The  $E_{miss}^x, E_{miss}^y$  are calculated in the laboratory frame. In practise instead of  $p_V^T$  and  $\phi$  the pair of variables  $p_V^T \cos \phi, p_V^T \sin \phi$  is used.

Notation	Features	Counts	Comments
True classification	Spin weights: $w_a, w_b$		Oracle predictions
Variant-All	4-vectors $(\pi^\pm, \pi^0, \nu)$	24/28/32	
Variant-1.0	4-vectors $(\pi^\pm, \pi^0)$	16/20/24	as in Table 3 of [8]
Variant-1.1	4-vectors $(\pi^\pm, \pi^0, \rho^\pm, a_1), m_i^2, m_k^2, y_i, y_k, \phi_{i,k}^*$	29/46/94	
Variant-2.0	4-vectors $(\pi^\pm, \pi^0), E_\nu, p_V^z, p_V^T$	22/26/30	True $E_\nu, p_\nu$
Variant-2.1	4-vectors $(\pi^\pm, \pi^0), E_\nu, p_V^z, p_V^T$	22/26/30	Approx. $E_\nu, p_\nu$
Variant-2.2	4-vectors $(\pi^\pm, \pi^0), E_\nu, p_V^z, p_V^T, E_{miss}^x, E_{miss}^y$	24/28/32	Approx. $E_\nu, p_\nu$
Variant-3.0.0	4-vectors $(\pi^\pm, \pi^0), E_\nu, p_V^z, p_V^T, \phi_\nu$	24/28/32	Approx. $E_\nu, p_\nu$ ; True $\phi_\nu$
Variant-3.1.4	4-vectors $(\pi^\pm, \pi^0), E_\nu, p_V^z, p_V^T, \phi_\nu$	24/28/32	Approx. $E_\nu, p_\nu$ ; Smeared $\phi_\nu$ ( $\beta=0.4$ )

Table 3: The AUC score achieved on the test sample by DNN trained on 25 epochs to discriminate between scalar and pseudo-scalar CP state of the Higgs boson. Results for  $\rho^\pm - \rho^\mp$ ,  $a_1^\pm - \rho^\mp$  and  $a_1^\pm - a_1^\mp$  decay modes are shown. Feature choice is labelled in the first column. For details see Table 2.

Features list	AUC ( $\rho^\pm - \rho^\mp$ )	AUC ( $a_1^\pm - \rho^\mp$ )	AUC ( $a_1^\pm - a_1^\mp$ )
True classification	0.782	0.782	0.782
Variant-All	0.764	0.739	0.692
Variant-1.0	0.655	0.596	0.557
Variant-1.1	0.655	0.601	0.558
Variant-2.0	0.661	0.619	0.569
Variant-2.1	0.657	0.608	0.562
Variant-2.2	0.657	0.608	0.563
Variant-3.0.0	0.752	0.717	0.654
Variant-3.1.2	0.744	0.709	0.654
Variant-3.1.4	0.724	0.685	0.623
Variant-3.1.6	0.701	0.662	0.604

constraints of the Higgs decay products. We show also how significant improvement will come with even very inaccurate, information on the azimuthal angle of neutrino directions.

We explore potential of classification with DNN technique with several variants of the feature lists, as detailed in Table 2. They are organised as family of Variant-X.Y, where X labels new category of features included and Y digit labels if their version is calculated from true 4-momenta or from approximations. The ultimate performance, labeled as True classification, is calculated using events spin weights  $w_A, w_B$ , where A, B denotes hypotheses for binary classification. It cannot be outperformed by the DNN with any Variant-X.Y. It may not be reached even with features list containing complete set of 4-momenta, denoted as Variant-All.

For the final performance we quote AUC score collected in Table 3 obtained on the test sample of simulated data (i.e. not used for training or validation) with DNN trained on 25 epochs. This was found as a most stable configuration which allows to compare different sets of Variant-X.Y. In the following subsections we discuss those results in some details.



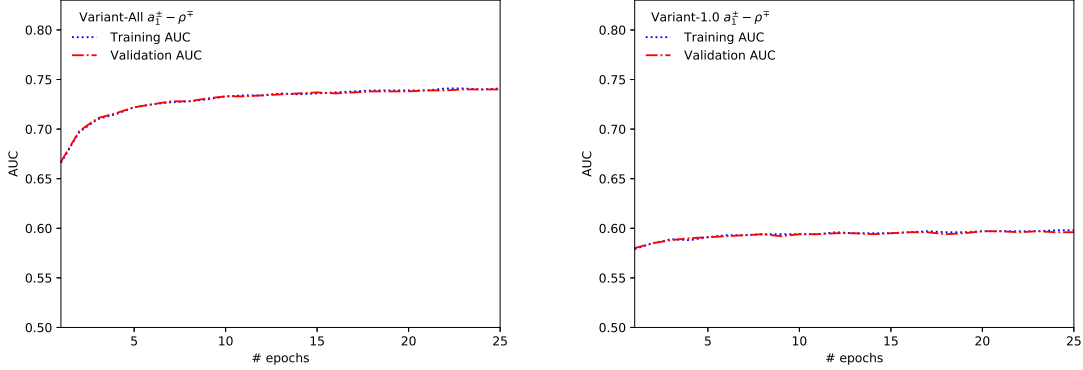


Figure 3: The AUC score on training and validation of  $a_1^\pm - \rho^\mp$  samples for list of features according to Variant-All (left plot) and Variant-1.0 (right plot) as a function of number of epochs.

#### 4.1 Benchmarks using all or only hadronic decay products

Results of Ref. [8], where only information on the visible decay products was used, have been summarised in Section 2 and Table 1. Nonetheless for overall consistency we present reevaluation of some of those results. The figures are prepared mainly for the  $a_1^\pm - \rho^\mp$  case, but in all other cases trends are quite similar.

For the first benchmark of DNN performance each event is represented with 4-vectors of all (including neutrinos) outgoing  $\tau$ -lepton decay products in the rest-frame of the hadronic decay products. This set of features is denoted as Variant-All. The results should reproduce optimal performance expected for the dataset (oracle predictions), with validation and training performance being consistent with each other. They are displayed in second line of Table 3. The oracle classification (AUC = 0.782) is not fully achieved. As we have verified it is mostly caused by dropout in the training procedure. In Fig. 3 (left plot) we show AUC score as a function of number of epochs used for training and validating, for the case of  $a_1^\pm - \rho^\mp$  channel. The highest achieved result on the validation sample is about 0.74.

As the second benchmark we use following Ref. [8], the same events but with features limited to 4-vectors of visible decay products of the  $\tau$  leptons together with other quantities which can be derived directly from them. The set of features with only 4-vectors of visible decay products in the respective rest-frames of intermediate resonances is denoted as Variant-1.0. They can be supplemented with the higher-level expert features like invariant masses of intermediate resonances or energy fractions, forming set of Variant-1.1. The achieved AUC results are collected in third and fourth lines of Table 3 for three decay modes and are very close for Variant-1.0 and Variant-1.1. Expert variables provides only redundant information. In Fig. 3 (right plot) we show AUC results for training and validation of  $a_1^\pm - \rho^\mp$  sample. The highest achieved result on the validation sample is about 0.60.

The large gap between AUC performance for the feature sets: Variant-All and Variant-1.0 is visible for all decay modes and we will try in the following to at least partially improve achieved performance, adding information on the neutrino momenta and in particular their azimuthal angles.

#### 4.2 Adding neutrino momenta

In this section we present improvements with the energy and longitudinal neutrino momenta. Such an extension of features list is not expected to be very beneficial as CP information is carried by the transverse degrees of freedom, but it may be helpful to optimize use of information derived from hadrons.

With assumptions as explained in Section 3, we approximate  $E_\nu$ ,  $p_\nu^z$ ,  $p_\nu^T$  for each of neutrinos in the rest-frame of hadronic decay products. It is interesting what is the impact of added information, i.e. true value of those neutrino components. From the 4-momenta of visible decay products only, we cannot access information of the individual  $p_\nu^x, p_\nu^y$  components. However, we can still add information of the  $E_{miss}^x, E_{miss}^y$  in the laboratory frame. It is redundant to some extent, it was used already for  $p_\nu^z$  from formula (6).

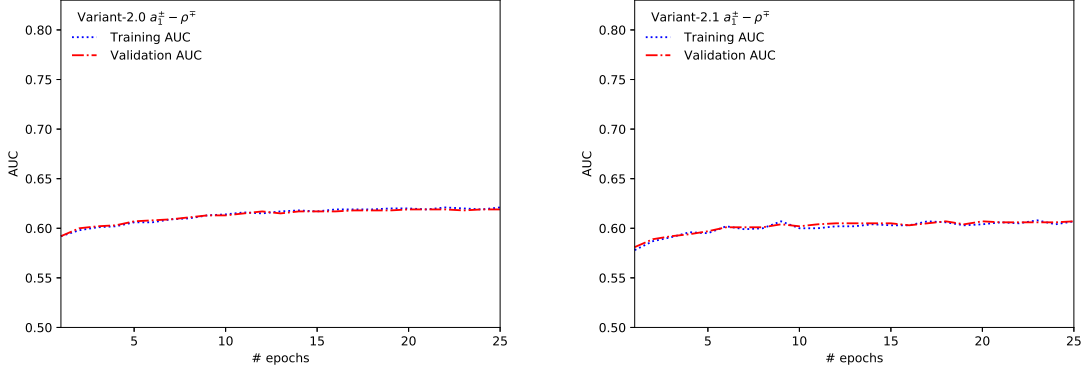


Figure 4: The AUC score on training and validation of  $a_1^\pm - \rho^\mp$  samples for list of features according to Variant-2.0 (left plot) and Variant-2.1 (right plot), as a function of number of epochs.

The augmented list of features, using true component of neutrino momenta, is denoted as Variant-2.0, while the ones using approximate components of neutrino momenta is denoted as Variant-2.1 and Variant-2.2, depending if the information on  $E_{miss}^x, E_{miss}^y$  is included or not. The achieved AUC scores by the DNN trained on 25 epochs are displayed in Table 3, for  $\rho^\pm - \rho^\mp$ ,  $a_1^\pm - \rho^\pm$  and  $a_1^\pm - a_1^\mp$  decay modes. Overall improvement from Variant-1.0 to Variant-2.0 is not very impressive. We observe small degradation of performance for Variant-2.1 with respect to Variant-2.0, which corresponds to the sensitivity lost due to approximate information on the neutrino features. The laboratory frame  $E_{miss}^x, E_{miss}^y$  Variant-2.2, are as expected of no help. In Fig. 4 we show ML performance for the  $a_1^\pm - \rho^\mp$  samples as a function of number of training epochs.

For feature sets: Variant-2.1 and Variant-2.2, three different approximations can be used to calculate  $E_\nu$ ,  $p_\nu^x$ ,  $p_\nu^y$ . The differences between *Approx-1*, *Approx-2* and *Approx-3* will certainly show up with detector effects included.

Clearly, the improvement from approximated information on the energy, longitudinal and module of transverse momenta of the neutrinos is rather small for all three decay modes. It indicates that the most sensitive information on the CP state lies in the azimuthal angle of the individual neutrinos in the transverse plane of hadronic decay products rest frames, i.e. individual  $p_\nu^x, p_\nu^y$  components and not  $p_\nu^T = \sqrt{(p_\nu^x)^2 + (p_\nu^y)^2}$ . Realistically any information on the individual  $p_\nu^x, p_\nu^y$  in the intermediate resonances rest frames could be reconstructed only if the measurement of the  $\tau$  decay vertices was possible. In the next Section we will evaluate how accurately this information has to be known to become useful. It constitute separate experimental challenge. Note that all other components of  $\nu_\tau$  momenta are reconstructed quite well from the measurable quantities. Detector smearing effects were not yet investigated though.

### 4.3 Azimuthal angles of neutrinos from decay vertices

The azimuthal angles  $\phi_{\nu_1}, \phi_{\nu_2}$  can be obtained from the measurement of the  $\tau$  lepton decay vertices. This is rather widely used technique in the experimental measurements, see eg. [26], but for  $\tau$ -mass or  $\tau$ -lifetime measurement rather than for neutrino azimuthal angles. But as it allows for complete reconstruction of the  $\tau$ -lepton momenta it can be used for our purpose as well.

Without any attempt to reconstruct those angles, we calculate them from the neutrinos 4-momenta, transformed to the rest-frames of the respective intermediate resonances and add to the features list forming sets denoted as Variant-3.0 and Variant-3.1.<sup>3</sup> The first one is for the true  $\phi_{\nu_1}^{true}, \phi_{\nu_2}^{true}$ , and second is for smeared  $\phi_{\nu_1}^{smeared}, \phi_{\nu_2}^{smeared}$ . In Fig. 5, left side, the distribution of  $\phi_{\nu_1}^{true} - \phi_{\nu_1}^{smeared}$  for  $\beta = 0.4, 0.8$  is given.

The ML results for AUC score are evaluated for  $\beta$  in the range  $[0, 2]$ . The AUC scores on the test samples for three decay modes are shown in Fig. 6 as a function of smearing parameter  $\beta$ . The AUC scores for  $\beta = 0.0$  reproduce, as they should, the ones of Variant-3.0 and are close to the scores of Variant-All. That is because

<sup>3</sup> The sub-subindex  $\beta$  encodes the size of the smearing parameter  $\beta$ .

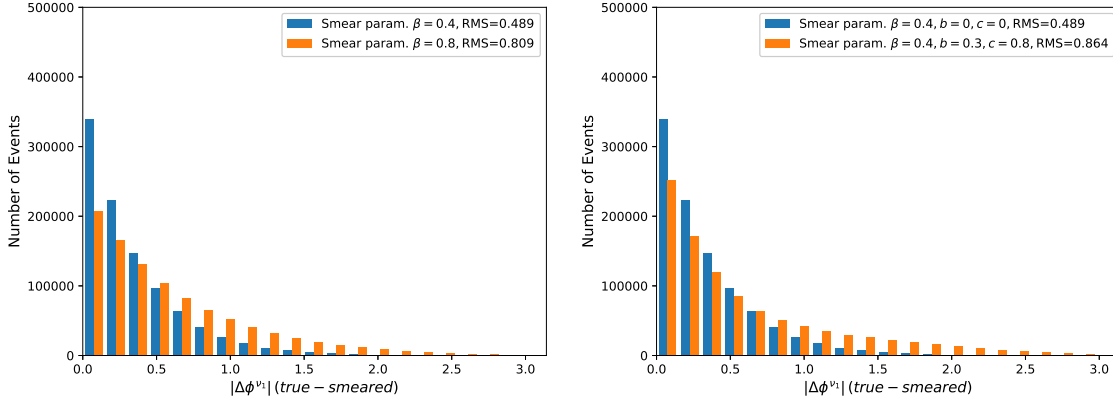


Figure 5: The  $\Delta\phi_{v1}$  (true - smeared) distribution for smearing parameter  $\beta=0.4, 0.8$  (left plot), and for  $\beta=0.4$  but with and without additional modulation with polynomial function (right plot).

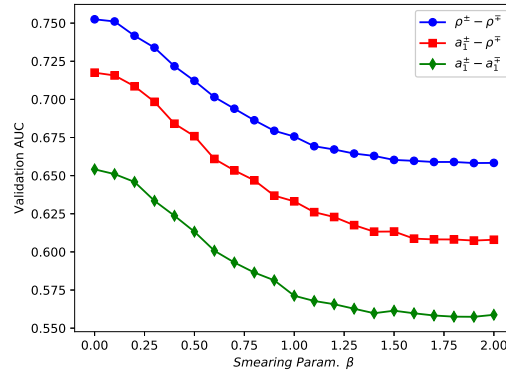


Figure 6: Plot of AUC score as a function of smearing parameter  $\beta$ , for  $\rho^\pm - \rho^\mp$ ,  $a_1^\pm - \rho^\mp$  and  $a_1^\pm - a_1^\mp$  decay modes.

the only difference is that approximate information on the longitudinal, transverse and energy components of the neutrino momenta were used. For higher values of  $\beta$ , above 1.4, the AUC scores decrease to the ones of Variant-2.1 sets, equivalent to not having information on the neutrino azimuthal angles at all. However estimate, even corresponding to rather large  $\beta = 0.4$  still contribute sizeably to CP Higgs sensitivity.

Derivative of sensitivity with respect to  $\beta$ , reach its maximum at about 0.35 and remains constant until  $\beta = 0.9$ . Then nearly all of the sensitivity due to the neutrino azimuthal angle is lost. For even larger  $\beta$  loss of sensitivity continues, but as the contribution is then small, deterioration is rather slow too.

Let us now study sensitivity of the ML algorithm to precise modeling of  $\phi_v$  angles resolution. We will assume that the resolution of the  $\phi_v$  reconstruction is not modeled well during the training procedure. For the validation sample we will introduce<sup>4</sup> additional component of the polynomial form for the smearing

$$f_{valid}(\Delta\phi_v, \beta, b, c) = \frac{1}{xnorm} \exp\left(-\frac{1}{\beta} \cdot \Delta\phi_v\right) (1 + b^2 \Delta\phi_v^2 + c^2 \Delta\phi_v^4). \quad (19)$$

These results mimic inefficiencies (mismodeling) of the sample used for DNN training, with respect to what is

<sup>4</sup>This polynomial function modification is implemented with the help of Monte Carlo unweighting with

$$wt = f_{valid}(\Delta\phi_v, \beta, b, c) / f_{train}(\Delta\phi_v, \beta). \quad (18)$$

and is used for validation and test samples.

Table 4: The AUC using Variant - 3.1. $\beta$  set of features for  $\rho^\pm - \rho^\mp$ ,  $a_1^\pm - \rho^\mp$  and  $a_1^\pm - a_1^\mp$  decay modes. The smearing parameter  $\beta = 0.2, 0.4$  and  $0.6$  is applied to training, validation and test sample. The test sample is additionally reweighted to introduce polynomial modifications to smearing function Eq. (19).

Parameters	AUC ( $\beta = 0.2$ )	AUC ( $\beta = 0.4$ )	AUC ( $\beta = 0.6$ )
	$\rho^\pm - \rho^\mp$		
$b = 0.0, c = 0.0$	0.744	0.724	0.701
$b = 0.3, c = 0.8$	0.741	0.678	0.617
$b = 0.9, c = 0.9$	0.738	0.665	0.611
	$a_1^\pm - \rho^\mp$		
$b = 0.0, c = 0.0$	0.709	0.685	0.662
$b = 0.3, c = 0.8$	0.707	0.638	0.569
$b = 0.9, c = 0.9$	0.704	0.627	0.565
	$a_1^\pm - a_1^\mp$		
$b = 0.0, c = 0.0$	0.654	0.623	0.604
$b = 0.3, c = 0.8$	0.645	0.580	0.537
$b = 0.9, c = 0.9$	0.640	0.576	0.532

present in the validation or test samples. In Table 4 we collected results for  $\rho^\pm - \rho^\mp$ ,  $a_1^\pm - \rho^\mp$ ,  $a_1^\pm - a_1^\mp$  cases, for  $\beta = 0.2, 0.4, 0.6$  and few choices of  $b$  and  $c$ . These results provide insight to boundary of ML capacity to use imprecise information. In Fig. 5, right side, the distribution of  $\phi_v^{true} - \phi_v^{smear}$  is given for  $\beta = 0.4$ , and  $b, c = 0.3, 0.8$ . For the left side plot  $b$  and  $c$  are set to 0. Table 4 summarises expected performance results for the case of  $a_1^\pm - \rho^\mp$  decay mode. The degradation is by far not critically large.

In our study, we have constrained directions of reconstructed neutrino momenta from kinematics, wherever expected precision of experimental inputs was better than that of impact parameters of decay vertices. Only remaining two angles used this rather low precision input. On the basis of Fig. 6 we can conjecture, that it is enough to reconstruct the approximate value of the  $\phi_v$  angle. Smearing with the shifts bigger than  $\frac{\pi}{4}$  or so, degrade sizably sensitivity only.

Such conjecture of existing critical size for the smearing to make  $\phi_v$  insensitive to CP, is of interest for any ML application. In case of  $\beta = 1.2$  for sizable fraction of events, the  $\Delta\phi_v$  was bigger than  $\frac{\pi}{4}$ . Then our ML solution did not demonstrate sensitivity gains from  $\phi_v$ . Still, may be, an approach relying less on  $\phi_v$  measurement, but on restriction, which events should be dropped from the analysis could be nonetheless useful. Possibly, for large smearing, elimination of events with high risk of  $\phi_v$  mis-reconstruction may be appropriate, as it was attempted in Ref. [17]. Discussion of physics properties simultaneously with those of the ML algorithms, may be again of interest.

## 5 Summary

Physics of CP parity measurement in  $H \rightarrow \tau\tau$  including  $\tau$  decays is rather simple from the perspective of theoretical modeling. Matrix element can be clearly defined. On the other side, parity effect manifest itself in rather complicated features of multi-dimensional distributions where kinematic constraints related to ultra-relativistic boosts play important role.

In our previous paper [8] we have studied performance of ML technique binary classification using information on the hadronic decay products of the  $\tau$  leptons only. Here we have turned our attention to neutrino momenta.

We have shown, how theoretical constraints of  $\tau$ -mass or  $H$ -mass and energy momentum conservation are essential to use whenever possible, instead of highly smeared information of neutrino kinematic from impact parameter. Resulting set of expert variables helps ML algorithms to establish measure of the distance between events, sensitive to physics requirements.

We have studied how partially reconstructed information on non-observable neutrinos can be used and which of physics constraints are helpful. Reconstructed with some approximation (using only visible decay products) longitudinal components of the neutrino momenta could improve AUC of 0.655, 0.601, 0.558 to about 0.657,

0.608, 0.563 respectively for  $\rho^\pm - \rho^\pm$ ,  $a_1^\pm - \rho^\mp$  and  $a_1^\pm - a_1^\mp$  cases. The improvement for sensitivity to Higgs boson CP-parity is rather minuscule, even without taking into account detector effects.

The more significant improvement would come, if the transverse components of the neutrino momenta were known, even imprecisely. This can be achieved if the  $\tau$ -lepton decay vertices are measured and used to reconstruct directions of the  $\tau$  leptons momenta. The performance of such reconstruction is detector specific. We have estimated how big improvement will be obtained if information is known with certain precision. This information, azimuthal angles  $\phi_\nu$  and  $\phi_{\bar{\nu}}$  even with large smearing, improve AUC from 0.675, 0.608 and 0.563 to about 0.724, 0.685 and 0.623 for  $\rho^\pm - \rho^\pm$  and  $a_1^\pm - \rho^\mp$  and  $a_1^\pm - a_1^\mp$  cases respectively. Note that  $\phi_\nu$  and  $\phi_{\bar{\nu}}$  angles represent intermediate step in the quest from expert variable to elementary features. We are leaving the topic of the angles measurements to the forthcoming work.

## Acknowledgments

P. Winkowska would like to thank L. Grzanka for valuable comments and suggestions through the time of preparing results of her MSc thesis at Department of Computer Science, AGH USiT.

## References

- [1] D. Guest, K. Cranmer, and D. Whiteson, 1806.11484.
- [2] P. Baldi, K. Bauer, C. Eng, P. Sadowski, and D. Whiteson, *Phys. Rev.* **D93** (2016), no. 9 094034, 1603.09349.
- [3] C. Shimmmin, P. Sadowski, P. Baldi, E. Weik, D. Whiteson, E. Goul, and A. Sjøgaard, *Phys. Rev.* **D96** (2017), no. 7 074034, 1703.03507.
- [4] D. Guest, J. Collado, P. Baldi, S.-C. Hsu, G. Urban, and D. Whiteson, *Phys. Rev.* **D94** (2016), no. 11 112002, 1607.08633.
- [5] G. Louppe, K. Cho, C. Becot, and K. Cranmer, 1702.00748.
- [6] P. Baldi, P. Sadowski, and D. Whiteson, *Nature Commun.* **5** (2014) 4308, 1402.4735.
- [7] P. Baldi, P. Sadowski, and D. Whiteson, *Phys. Rev. Lett.* **114** (2015), no. 11 111801, 1410.3469.
- [8] R. Jozefowicz, E. Richter-Was, and Z. Was, *Phys. Rev.* **D94** (2016), no. 9 093001, 1608.02609.
- [9] I. Goodfellow, Y. Bengio, and A. Courville, *Deep learning*. MIT Press, Cambridge, MA, 2017.
- [10] G. R. Bower, T. Pierzchala, Z. Was, and M. Worek, *Phys. Lett.* **B543** (2002) 227–234, hep-ph/0204292.
- [11] T. Przedzinski, E. Richter-Was, and Z. Was, *Eur. Phys. J.* **C74** (2014), no. 11 3177, 1406.1647.
- [12] E. Barberio, B. Le, E. Richter-Was, Z. Was, D. Zanzi, and J. Zaremba, *Phys. Rev.* **D96** (2017), no. 7 073002, 1706.07983.
- [13] J. H. Kuhn, *Phys. Rev.* **D52** (1995) 3128–3129, hep-ph/9505303.
- [14] ATLAS Collaboration, M. Aaboud *et al.*, 1811.08856.
- [15] ATLAS Collaboration, G. Aad *et al.*, *JINST* **11** (2016), no. 04 P04008, 1512.01094.
- [16] A. Rouge, *Phys. Lett.* **B619** (2005) 43–49, hep-ex/0505014.
- [17] K. Desch, Z. Was, and M. Worek, *Eur. Phys. J.* **C29** (2003) 491–496, hep-ph/0302046.
- [18] S. Berge, W. Bernreuther, and S. Kirchner, *Phys. Rev.* **D92** (2015) 096012, 1510.03850.
- [19] P. Baldi, K. Cranmer, T. Faucett, P. Sadowski, and D. Whiteson, *Eur. Phys. J.* **C76** (2016), no. 5 235, 1601.07913.

- [20] T. Chen and C. Guestrin, 1603.02754.
- [21] L. Breiman, *Machine Learning* **45** (2001), no. 1 5–32.
- [22] A. Bevan, R. Goni, and T. Stevenson, *J. Phys. Conf. Ser.* **898** (2017), no. 7 072021, 1702.04686.
- [23] A. P. B. Bradley, *Pattern recognition* **30** (1997) 1145.
- [24] T. Fawcett, *Pattern Recognition Letters* **27** (2006), no. 7 861.
- [25] K. Desch, A. Imhof, Z. Was, and M. Worek, *Phys. Lett.* **B579** (2004) 157–164, hep-ph/0307331.
- [26] D. Jeans, *Nucl. Instrum. Meth.* **A810** (2016) 51–58, 1507.01700.
- [27] M. Abadi, A. Agarwal, P. Barham, E. Brevdo, Z. Chen, C. Citro, G. S. Corrado, A. Davis, J. Dean, M. Devin, *et al.*, *Software available from tensorflow.org* **1** (2015).
- [28] D. Kingma and J. Ba, *arXiv:1412.6980* (2014).
- [29] S. Ioffe and C. Szegedy, *arXiv:1502.03167* (2015).
- [30] N. Srivastava, G. E. Hinton, A. Krizhevsky, I. Sutskever, and R. Salakhutdinov, *Journal of Machine Learning Research* **15** (2014), no. 1 1929–1958.
- [31] A. F. Agarap, *arXiv:1803.08375* (2018) 1803.08375.
- [32] M. Fernandez-Delgado, E. Cernadas, S. Barro, and D. Amorim, *Journal of machine learning Research* **15** (2014) 3133–3181.
- [33] C. Zhang, L. Changchang, Z. Xiangliang, and G. Almpnanidis, *Expert Systems with Applications* **82** (2017) 128.
- [34] Pedregosa F. and et all, *Journal of Machine learning Research* **12** (2011) 2825.
- [35] T. Oshiro, P. Perez, and J. Baranauskas, “How many trees in a random forest?”, in *International Workshop on Machine Learning and Data Mining in Pattern Recognition, Springer, Berlin, Heidelberg*, 2012.
- [36] Prometheus computing cluster, Academic Computing Centre CYFRONET, Krakow, Poland.

## A Deep Learning Neural Network

The structure of the simulated data and the DNN architecture follows what was published in our previous paper [8]. It is based on TensorFlow [27], an open-source framework for numerical computations. Learning procedure is optimized using a variant of stochastic gradient descent algorithm called Adam [28]. We also use a recent ideas called Batch Normalization [29] and Dropout [30] to improve the training of the DNN. The problem of determining Higgs boson CP state is framed as binary classification because the aim is to distinguish between the two possible Higgs CP states.

We use the same samples of simulated data and start from the code published in [8]. Let us remind therefore only briefly few technical points on the used DNN implementation. We consider three separate problems for  $H \rightarrow \tau^\pm \tau^\mp$  decay modes:  $\rho^\pm - \rho^\mp$ ,  $a_1^\pm - \rho^\mp$ ,  $a_1^\pm - a_1^\mp$ . We solve all three problems using the same neural network architecture. Depending on the decay modes of the outgoing  $\tau$  pairs each of the cases contains different number of dimensions to describe an event, i.e. production of the Higgs boson decaying into  $\tau$  lepton pair. Each data point consists of features, which represent the observables/variables of consecutive event. The data point is thus an event of the Higgs boson production and decay into  $\tau$  lepton pair. The structure of the event is represented as follows:

$$x_i = (f_{i,1}, \dots, f_{i,D}), w_{a_i}, w_{b_i} \quad (20)$$

The  $f_{i,1}, \dots, f_{i,D}$  represent numerical features and  $w_{a_i}, w_{b_i}$  are weights proportional to the likelihoods that an event comes from a set  $A$  or  $B$  (the problem is framed as binary classification). The weights calculated from the quantum field theory matrix elements are stored in the simulated data files. This is a convenient situation, which does not



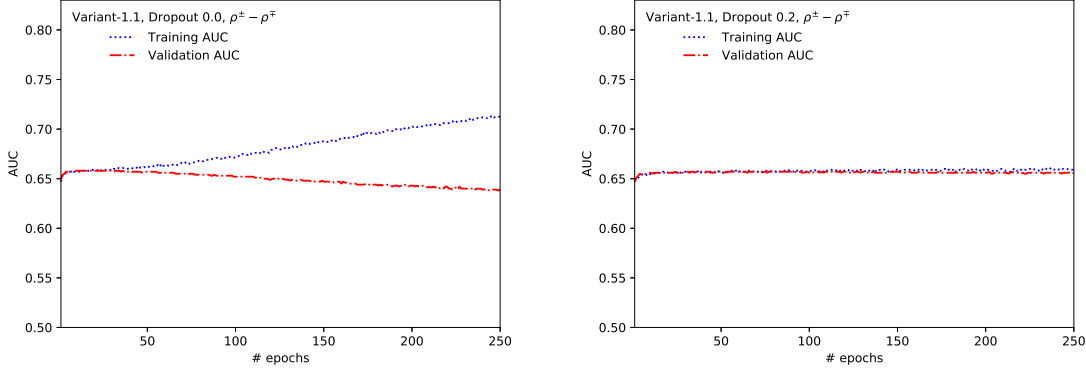


Figure 7: The AUC distribution for DNN training and validation for Variant-1.1 of  $\rho^\pm - \rho^\mp$  sample. Without dropout (left-plot) and with dropout = 0.2 (right-plot).

hold in many other cases of ML classification. The  $A$  and  $B$  distributions highly overlap in the  $(f_{i,1}, \dots, f_{i,D})$  space, more detailed discussion can be found in [8]. The perfect separation is therefore not possible and  $w_{a_i}/(w_{a_i} + w_{b_i})$  corresponds to the Bayes optimal probability that an event is sampled from set  $A$  and not  $B$ . The  $w_{a_i}, w_{b_i}$  are used to compute targets during the training procedure.

Thanks to the fact that model  $A$  and  $B$  are prepared using the same sample of events, but only with different  $w_{a_i}, w_{b_i}$  (the spin weight), the statistical fluctuations are largely reduced in the learning procedure. It has also consequences on actual implementation of the ML metric and code.

To quantify classification performance, weighted Area Under Curve (AUC) [23, 24] is used. For each data point  $x_i$ , the DNN returns probability  $p_i$  that it is correctly (not correctly) classified as of type  $A$ , and it contributes to the final loss function twice, with weight  $w_{a_i}$  ( $w_{b_i}$ ) respectively. With this definition, the  $AUC = 0.5$  would be obtained for random assignment, while the  $AUC = 1.0$  would be reached for perfect separation of the distributions. As in the studied problems distributions are overlapping, the best achievable  $AUC \simeq 0.782$  is reached with optimal predictions  $p_i = w_{a_i}/(w_{a_i} + w_{b_i})$  (oracle predictions). It depends slightly on the case studied.

Use of weighted events with  $w_a, w_b$  is for implementation convenience and to limit statistical fluctuations. We have repeated some of the DNN classification chain (training, validation, testing) using unweighted events<sup>5</sup>. We have found very good consistency of achieved in this way performance.

The DNN architecture used consists of  $D$ -dimensional input (list of features) followed by six layers of 300 nodes each with ReLU [31] activation functions and 1-dimensional output layer returning  $p_i$  probability between two choices, calculated using softmax function. The metric minimized by the model is negative log likelihood of the true targets under Bernoulli distributions.

The parameter which was optimised, with respect to what was used in [8], was a dropout [30]. For analysis presented in Ref. [8] AUC performance was obtained after training with 5 epochs. It was considered sufficient. Here, given variety of feature lists, we performed training on much larger number of epochs and studied what would be the optimal working point for number of epochs and dropout. The dropout = 0.20 seemed the optimal choice, to avoid overfitting in case of larger number of training epochs. The best performance was achieved after 5-25 epochs, depending on the case. Training with 25 epochs was used on the test samples to quote final AUC performance. While optimising threshold on dropout, we have observed that although it leads to more robust trained DNN (smaller risk for overfitting) the performance was sometimes slightly reduced. Positive impact of dropout is illustrated in Fig. 7 of Variant-1.1 training and validation for  $\rho^\pm - \rho^\mp$  case.

## B Alternative ML techniques

Although Deep Learning Neural Network is often used for classification tasks in High Energy Physics, many other more classical techniques are used as well, and often are able to achieve similar classification performance.

<sup>5</sup>Randomly sampling with respective weights distributions for model  $A$  and  $B$  and only then training DNN on those events.

Despite promising results that are often enlisted in papers, one should always remember that a Machine Learning technique that could perform well on one dataset with specific features, may deliver not so promising results on the other tasks.

The arguments of more fundamental nature, resulting from the investigations of mathematical assumption behind particular ML libraries, can be provided. The solutions which were chosen in libraries depend on the application domains the particular systems were prepared for. The Ref. [32] can be used as a guidance in that direction. Recent study [33] collected very extensive comparison of several Machine Learning algorithms. We will not contribute to that topic directly. However, in the following studies we will show that indeed it is the case for applications discussed through this paper. For our cases DNN technique turns out to be by far outstanding the performance of the more classical ones.

The following three Machine Learning techniques were chosen for the comparative study:

- *Boosted Trees* (BT) [20]
- *Random Forest* (RF) [21]
- *Support Vector Machine* (SVM) [22]

For *Boosted Trees* the XGBoost [20] library was used, while for *SVM* and *Random Forest* the `scikit-learn` [34] was chosen.

In the comparison of ML methods the AUC score was used as a performance measure. This is one of the recommended approaches when using a single number in evaluation of Machine Learning algorithms on binary classification problems. To make sure that the results are unbiased, the comparison was carried out on the same datasets<sup>6</sup> (including the division into training and validation parts).

For the *Boosted Trees* method the point of interest was to check the dependence of depth of tree and obtained results. More levels to the tree affects complexity of computation, a search for optimal value in terms of both achieved result and complexity of computation was performed. Suggested values for tree depth for *Boosted Trees* are between 3 and 10. First we have used depths 3 to 20. The upper bound was increased to better see the trend on plots of AUC score for classifiers depending on depth. The results seemed to rise up until depth 20, one more evaluation was added for depth equal to number of features in a given `Variant-X.Y` list. The AUC score for *Boosted Trees* classifier depends on the depth of the tree, see Fig. 8 for the  $\rho^\pm - \rho^\mp$  case and several variants of the feature list.

As suggested in the literature [35], for the *Random Forest* method, a baseline of the 128 trees (estimators) in the forest were used. For the next best split during the tree building number of features equal to  $\log_2(N_f)$  or  $\sqrt{N_f}$ , where  $N_f$  denotes number of features, was tried. Performance was comparable. For depth of the trees the one optimal for *Boosted Trees* was used. The tests with larger number of trees (300) and tree depths (30) were also carried out, see Fig. 8.

For the *Support Vector Machines* method first tests were performed to check which kernel: linear or rbf could give more promising results. The rbf kernel was chosen because of better stability of results and then fine-tuning of  $C$  and  $\gamma$  parameters (soft margin and kernel parameters) was performed. The parameters evenly distributed on logarithmic scale between  $10^{-3}$  and  $10^3$  were tested. To avoid excessive computation, the stage of fine-tuning was performed on only one feature list, namely *Variant-All* and on smaller sample. These parameters ( $C = 10$  and  $\gamma = 0.1$ ) were then used to train *SVM* on other feature lists as well.

The comparison of achieved best performance for the case of  $\rho^\pm - \rho^\mp$  decay mode and different variants of the feature lists is shown in Table 5. Clearly performance of the *DNN* is outstanding for all considered variants. One can also notice the trend that while performance is slightly improving when moving from *Variant-1.0* to *Variant-2.1* for *DNN* method, it starts deteriorate for other ML techniques.

We have performed comparisons of the execution time, memory usage and efficiency too. At the *Prometheus* cluster [36], we have executed jobs at 1 node with 4 tasks per node and 5GB memory per task. The comparison is reported in Table 6. The achieved AUC by *DNN* is by far outstanding other ML techniques. The other ones, among themselves, gave comparable performances. The *SVM* training took by far the longest time. Training of *BT* took the least time, under 10 minutes, which was 8 times less than for *DNN*. Both *DNN* and *RF* used the resources efficiently, achieving efficiency of 68.8% and 96.1% respectively.

---

<sup>6</sup> In case of SVM subsets were used.

Table 5: AUC score for different ML methods used on the validation sample and  $\rho^{\pm} - \rho^{\mp}$  decay mode.

Features set	DNN	BT	RF	SVM
Variant-All	0.764	0.641	0.626	0.635
Variant-1.0	0.655	0.569	0.567	0.559
Variant-2.1	0.657	0.564	0.564	0.572
Variant-2.2	0.657	0.562	0.559	0.568

Table 6: The benchmark AUC score for different methods of the  $\rho^{\pm} - \rho^{\mp}$  training sample with the Variant-1.0 features. Time of training, memory usage and efficiency information, as reported by job submission queue system is given. The training on 800k data points for DNN, BT and RF methods was performed. For the SVM 100k data points were used.

Method	# Data points	AUC	Time of training (h:min:sec)	Memory usage (% of 20GB)	Efficiency (CPU)
Deep Neural Network	800 k	0.644	01:21:58	6.3%	68.8%
SVM	100 k	0.572	01:52:03	4.3%	25.0%
Boosted Decision Trees	800 k	0.571	00:09:40	9.6%	24.9%
Random Forest	800 k	0.569	00:34:25	37.9%	96.1%

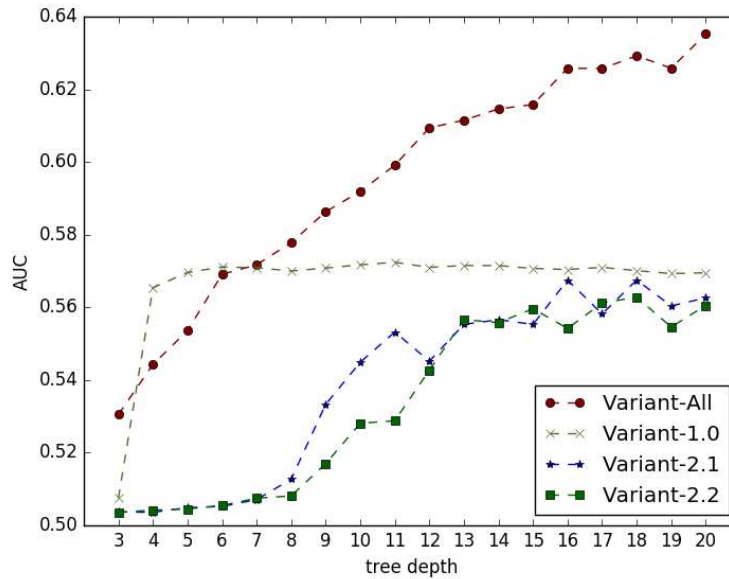


Figure 8: The AUC score achieved with *Boosted Trees* classifier depending on the depth of the tree.